IEEJ TRANSACTIONS ON ELECTRICAL AND ELECTRONIC ENGINEERING
IEEJ Trans 2017; **12**(S1): S54–S64
Published online in Wiley Online Library (wileyonlinelibrary.com). DOI:10.1002/tee.22439

Paper

Optimal Coordination of Voltage Controllable Devices in Distribution Systems using Power-based Models and Quadratic Programming

Tu Van Dao*, Non-member
Surachai Chaitusaney*[a], Member
Yasuhiro Hayashi**, Member
Hideo Ishii**, Member

The incorporation of photovoltaic (PV) inverters makes the management of voltage difficult for power system operators. One solution is to consider these inverter-based devices as controllable reactive power (VAr) sources and to coordinate them with other voltage regulating devices in the distribution system. This paper proposes some acceptable approximations to quickly formulate and solve a mixed-integer quadratic programming problem to periodically determine the optimal voltage coordination of a load tap changer, voltage regulators, capacitor banks, and PVs on a smart grid platform. The solution to the optimization problem is aided by an iteration-based algorithm. By using the MATLAB software to carry out the simulation and computation, the method is well verified by comparing its generated result with a trustworthy solution obtained from examining all possible coordinating combinations of voltage regulating devices and PVs in a modified IEEE 34-bus system. The effectiveness and features of the method are clearly illustrated on that test system by considering a time-varying load and PV generation. The obtained results demonstrate the practical application of this work to medium-voltage systems. © 2017 Institute of Electrical Engineers of Japan. Published by John Wiley & Sons, Inc.

Keywords: distribution systems; load tap changers; photovoltaics; quadratic programming; volt/var control

Received 1 June 2016; Accepted 5 February 2017

1. Introduction

Traditionally, power utilities use their own devices to manage the supply voltage. Typical equipment for controlling the voltage in medium-voltage networks includes load tap changers (LTCs) at the substation, downstream voltage regulators (VRs), and capacitor banks (CBs). In addition, photovoltaic (PV) inverters can be considered as voltage regulating devices because they are highly capable of controlling the reactive power. Furthermore, the widespread installation of PVs in distribution systems is challenging power companies to provide an effective solution to manage the system voltage.

With the advent of two-way communication and real-time measurement, including advanced metering infrastructure (AMI), voltage can be controlled on a real-time basis in a central control structure. The authors in [1] tested a rule-based control so that voltage regulating devices were sequentially adjusted until feedback voltages were brought back to within limits. With the assumption of high computational efficiency of the distribution management system (DMS), the authors in [2,3] proposed an online control strategy based on real-time and pseudo measurements for running a state estimator and then the tuning parameters to update all voltage regulating devices including distributed generations.

When taking some features of a smart grid such as the high performance of communications and the computing capability into account, coordination of all voltage regulating devices can be optimized by considering the slow fluctuation of load and PV generation throughout the day. Generally, there are two obstacles to be addressed when controlling the voltage: prediction of the system condition, and the speed of finding the optimal coordination for real-time control. The authors of [1] also proposed a mixed-integer nonlinear programming (MINLP) problem, but they also pointed out that the execution time would be too long if a large number of discrete control variables are involved.

Up to now, several voltage control schemes have been proposed to deal with the aforementioned obstacles. In [4], load and PV generation for the next short time are predicted to pick up the optimal parameters for the line drop compensator (LDC) from a set of classifiers. A similar approach is employed in [5] for dynamically updating the control parameters of multiple advanced step VRs. Based on the same idea of using a database, the approach in [6] requires real-time measurements instead of forecast data. In [7,8], the authors evaluated all possible critical scenarios to employ a rule of thumb for the variable settings of voltage setpoint and bandwidth of the LDC. A synthesis of these methods is that settings of the devices are dynamically adjusted using a ready database so that the new parameters are quickly selected and the upcoming system condition is expected to be considered.

This paper proposes a novel method to optimally coordinate all voltage regulating devices on the smart grid platform. By linearizing the model of the whole system, the changes of discrete variables (tap positions and CB switching states) are modeled as continuous power adjustments for implementing a quadratic programming (QP) problem. Thus, the computational time is reduced significantly. In addition, the number of operations of LTCs, VRs, and CBs is reduced by adding an appropriate set of weighting factors into the objective function (OF) of the formulated optimization.

[a] Correspondence to: Surachai Chaitusaney.
E-mail: surachai.c@chula.ac.th

*Department of Electrical Engineering, Faculty of Engineering, Chulalongkorn University, Bangkok 10330, Thailand
**Advanced Collaborative Research Organization for Smart Society (ACROSS), Waseda University, Tokyo, Japan

The remainder of the paper is organized as follows. Section 2 introduces a structure of two-layer voltage control in distribution systems. Section 3 summarizes and adapts models of devices in medium-voltage networks to prepare a basis for formulating a voltage control problem. The controlling method of the first layer is presented in Section 4, where a mixed-integer QP method embedded in an algorithm to improve the accuracy of the solution is proposed. The next section presents a method of fast control in the second layer to cope with sudden changes in PV active power output. Section 6, as a case study, employs a standard IEEE test system to verify the proposed method. The last section summarizes the main contents and includes some concluding remarks as well.

2. Two-Layer Voltage Control Structure

A general structure of a voltage control scheme with AMIs and field remote terminal units (FRTUs) feedback, which is adopted from the Japan National Project [9], is shown in Fig. 1. The same structure has been also employed widely, e.g. in [10,11]. It basically comprises two layers as follows:

2.1. Long timescale control

This layer optimizes the coordination periodically, e.g. every 1 h or 15 min. Therefore, a central controller installed at the utility control center can successfully carry out the voltage control scheme. After solving an optimization problem, it determines the settings of all devices and sends control signals to the field equipment. Compared to the method in [11], which solves the MINLP directly, the proposed method in this paper is faster and more effective as illustrated in the Case Study section.

The proposed method is truncated at the primary side of the Medium-voltage/ Low-voltage transformers (service transformers), similar to the approach in [12,13]. Based on the smart meters' capability of capturing current and voltage waveforms, the aggregated load can be estimated accurately enough; roof-top PVs on each low-voltage side are also aggregated and forecast for the concerned period. In the future, the low-voltage side with high penetration of roof-top PVs might be controlled by its own system and would be integrated into the proposed method via a multi-agent-based structure.

2.2. Short timescale control

During the specified time ahead (set by the long timescale layer), a short timescale control located on each inverter control system takes the responsibility for mitigating the voltage fluctuation due to fast changes in the PV output. When a PV detects a reduction in its output compared to the forecast value, the VAr required by the long timescale control is temporarily neglected and the PV is switched into a fast control mode. The optimal VAr is ignored just in a short duration until the watts output turns back to the expected (forecast) value. Afterward, the reactive power is set to the optimal one as usual.

In this paper, a compensation factor (K_{QP}) is proposed to control the reactive power of the PV so that the injection of VAr is sufficient to retain the expected voltage in the case of a sudden active power reduction due to moving clouds. Each K_{QP} of a PV is optimized by the controller for the same period in the long timescale control. This is different from the method in [11], which performs thousands of power flows to approximate power–voltage sensitivities.

3. Power-based Models of System Components

This section summarizes and proposes some adaptations when modeling load and voltage regulating devices based on an idea of power adjustment. The obtained models will be utilized for formulating a voltage control problem.

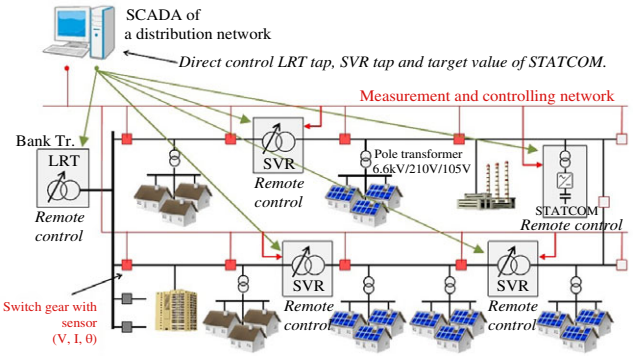

Fig. 1. Configuration of the centralized voltage control [9]. LRT, load ratio transformer ≡ LTC; SVR (step voltage regulator) ≡ VR]

3.1. Load model

Traditionally, a load can be modeled as a constant-power, a constant-current, or a constant-impedance value. Equations (1) and (2) are used to express those models:

$$P = P_0 \begin{bmatrix} Z_p & I_p & P_p \end{bmatrix} \begin{bmatrix} (V/V_0)^2 & V/V_0 & 1 \end{bmatrix}^T \quad (1)$$

$$Q = Q_0 \begin{bmatrix} Z_q & I_q & P_q \end{bmatrix} \begin{bmatrix} (V/V_0)^2 & V/V_0 & 1 \end{bmatrix}^T \quad (2)$$

where the subscript 'T' stands for the transpose of a vector, and P_0 and Q_0 are the active and reactive power consumption at the rated voltage (V_0). The coefficients satisfy the conditions ($Z_p + I_p + P_p = 1$) and ($Z_q + I_q + P_q = 1$) to ensure that the load model consumes the rated power at its rated voltage. Some combinations of [Z, I, P] are examples of the traditional model: [0 0 1] for constant-power load, [0 1 0] for constant-current load, and [1 0 0] for constant-impedance load. In addition, a more accurate model with other combinations of [Z, I, P] is also introduced in [14,15].

3.2. Voltage regulating devices

Common devices for voltage regulation in medium-voltage networks are LTC transformers, VRs, and CBs. Recently, grid-connected generators such as PVs and wind turbines have been employed for supporting the voltage, so they can also be considered as voltage regulating devices.

3.2.1. LTC transformer and VR An LTC transformer is usually located at the substation and modeled by a circuit of a branch admittance in series with an ideal transformer. For brevity of expression, an LTC transformer is referred to as 'LTC' hereafter. To simulate the control actions of an LTC during power flow, a fictitious injection current was proposed by Roytelman and Ganesan [16]. This idea was then utilized in [17,18] for the three-phase power flow calculation. Since phase-shifting transformers are usually employed in transmission systems to control the active power flow [19], they are out of the scope of this paper. An LTC can be modeled by an ideal transformer at a ratio (t) in series with an admittance ($y = g + jb$), as depicted in Fig. 2(a), where t is considered a real number and remains unchanged when taking the conjugate, i.e. $t^* = t$.

The relationship between the current and the voltage after moving from a transformer ratio t to $T = t + \Delta t$ is given by (3) and shown in Fig. 2(b) [16]. The additional currents detached from (3) are considered as two fictitious current sources defined by (4), and they flow out of buses h and k. In this paper, these current sources are converted into two power sources injected into these buses by using the corresponding voltage. Accordingly, the additionally injected complex power sources are given by (5) and (6), where

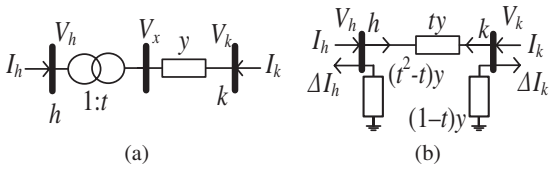

(a) (b)

Fig. 2. LTC model: (a) Transformer with ratio 1:t . (b) Π model at ratio $T = t + \Delta t$

$\Delta\delta_{kh} = \delta_k - \delta_h$ and $\Delta\delta_{hk} = -\Delta\delta_{kh}$, with δ_k and δ_h being the angles of V_k and V_h, respectively.

$$\begin{bmatrix} I_h \\ I_k \end{bmatrix} = \begin{bmatrix} t^2 y & -ty \\ -ty & y \end{bmatrix} \begin{bmatrix} V_h \\ V_k \end{bmatrix} + \begin{bmatrix} \Delta I_h \\ \Delta I_k \end{bmatrix} \tag{3}$$

$$\begin{bmatrix} \Delta I_h \\ \Delta I_k \end{bmatrix} = \begin{bmatrix} \Delta ty\,[(2t + \Delta t)\,V_h - V_k] \\ -\Delta ty\,V_h \end{bmatrix} \tag{4}$$

$$\begin{aligned} \Delta S_k &= -V_k(-\Delta ty\,V_h)^* = \\ &\Delta t|V_k||V_h|(g\cos\Delta\delta_{kh} + b\sin\Delta\delta_{kh}) + \\ &j\,\Delta t|V_k||V_h|(g\sin\Delta\delta_{kh} - b\cos\Delta\delta_{kh}) \end{aligned} \tag{5}$$

$$\begin{aligned} \Delta S_h &= \Delta t|V_h|\{g|V_k|\cos\Delta\delta_{hk} - \\ &(2t + \Delta t)g|V_h| + b|V_k|\sin\Delta\delta_{hk}\} + \\ &j\,\Delta t|V_h|\{g|V_k|\sin\Delta\delta_{hk} - \\ &b|V_k|\cos\Delta\delta_{hk} + b|V_h|(2t + \Delta t)\} \end{aligned} \tag{6}$$

Generally, an LTC is constructed with off-LTCs in the high-voltage side winding and on-LTCs in the low-voltage side. For frequent voltage control actions, taps on the low-voltage side are adjusted. If the off-load tap is at the nominal position, the relationship between tap position (Tap) and transformer ratio (t) of the on-LTCs is like the one for VRs below.

A VR can be viewed as a tap-changing autotransformer with very small series impedance and shunt admittance. Thus, they are neglected in a VR model, so that the VR is treated as an ideal transformer in the power flow algorithm. Consequently, the nodal admittance matrix becomes infinite due to zero-impedance branches. This infinity is avoided by merging the zero-impedance branch with the adjacent branches to formulate new nonzero-impedance branches [20]. Such a representation is like an LTC model. Hence, the above idea of injecting additional complex power sources can be applied to model the tap movement of a VR.

Step VRs can be defined as type A or B depending on which side the taps are located at. Type A is arranged with tapped series winding on the load side, and type B has taps on the source side. Generally, a standard VR has 32 tap positions, excluding the nominal tap (tap zero). Accordingly, each incremental step varies by 0.625%. If Tap is numbered from −16 to +16, the relationship between Tap and t is given by (7) for a type B VR, which is predominantly used for downstream feeders than type A. In this equation, Tap with the minus sign indicates a 'lower' position and the positive one indicates a 'raise' position.

$$t = 1 + 0.00625 \times \text{Tap} \quad (\text{Tap} = -16, \ldots, 16) \tag{7}$$

3.2.2. Capacitor bank In order to retain the consistency of the nodal admittance matrix, a CB should be represented by a reactive power source computed from the voltage (V_C) and the capacitive reactance (Z_C), which depends on how many banks are switched on. If each bank of a multistep CB is switchable by a switch S_C ($S_C = 0, 1, \ldots, N_{\text{bank}}$), the reactive power source is given as (8), where Q_C is non-negative; when $S_C = 0$ (the CB is fully opened), $Q_C = 0$. In the case of a single-step CB, S_C has only two values: $S_C = 0$ and $S_C = 1$.

$$Q_C = \begin{cases} V_C^2/(S_C Z_C) & \text{if } S_C \neq 0 \\ 0 & \text{if } S_C = 0 \end{cases} \tag{8}$$

3.2.3. PV plant Grid-connected PVs are considered here because of their widespread installation and their capability to quickly control the reactive power and the fine resolution on the VAr output. At specified active and reactive power values, a PV can be treated as a PQ node for running the power flow calculation. It is thus possible to model a PV by an adjustable VAr source ΔQ_{pv} during voltage regulation. Physically, the reactive power must not be greater than a capability $Q_{\text{pv max}}$ with respect to the currently generating active power P_{pv} and the fixed maximum apparent power $S_{\text{pv max}}$. However, if we assume that a PV is required to adjust the reactive power only during daytime when it generates active power and that the power factor (cos ϕ) must not less than 0.85, the limitation of the reactive power of a PV can be given as (9). In this equation, $0.62P_{\text{pv}}$ is the limitation corresponding to the power factor of 0.85.

$$|Q_{\text{pv}}| \leq Q_{\text{pvmax}} = \text{Min}\{0.62P_{\text{pv}};\ \sqrt{S_{\text{pvmax}}^2 - P_{\text{pv}}^2}\} \tag{9}$$

3.2.4. Power flow algorithm A good method to avoid the divergence of a power flow algorithm in radial networks is current injection based on the backward/forward technique. A sweeping process is repeated until a predefined stopping criterion is satisfied. Both its performance and how many times it is mobilized by the optimization process play a key role in reducing the time to reach the optimal coordination and, hence, the responding speed of the real-time control.

4. MINLP for Voltage Control in the Long Timescale

The long timescale layer periodically formulates an optimization problem and solves it to determine the optimal settings of all control devices. This section first presents a general voltage control problem solved by an MINLP solver and then introduces some approximations to change the problem to a QP one and solves it by the proposed method.

4.1. Formulation of an MINLP for voltage control

The voltage control problem can be formulated as an MINLP form (10) used widely in the literature [1,11]:

$$\begin{aligned} &\text{Min}\, f(x, u_{\text{d}}, u_{\text{c}}) \\ &g(x, u_{\text{d}}, u_{\text{c}}) = 0 \\ &h(x, u_{\text{d}}, u_{\text{c}}) \leq 0 \end{aligned} \tag{10}$$

where x is the vector of dependent variables (voltages), u_{d} is the vector of discrete variables (tap positions, CB switching states), and u_{c} is the vector of continuous variables (PV power). Details of the optimization model is as follows:

4.1.1. MINLP objective function As stated in the introductory section, the number of tap changes per day of the voltage regulating devices is expected to be a minimum. In addition, the distance of moving the tap position each time should be as short as possible to prevent any sudden voltage change at load points near the LTC or VR. We approach the problem by minimizing the moving distance of the tap from the

initial state. In this approach, the OF, given by (11), can be considered.

$$\mathrm{Min}\left[W_\mathrm{P}\sum_{i=1}^{N_\mathrm{P}}\left(Q_{\mathrm{pv}0i}+\Delta Q_{\mathrm{pv}i}\right)^2 + W_\mathrm{R}\sum_{k=1}^{N_\mathrm{R}}\left(\Delta\mathrm{Tap}_{\mathrm{R}k}\right)^2 + W_\mathrm{C}\sum_{j=1}^{N_\mathrm{C}}\left(\Delta S_{\mathrm{C}n}\right)^2\right] \tag{11}$$

In (11), $\Delta\mathrm{Tap}_{\mathrm{R}k}=|\mathrm{Tap}_{\mathrm{R}k}-\mathrm{Tap}_{0\mathrm{R}k}|$ and $\Delta S_{\mathrm{C}n}=|S_{\mathrm{C}n}-S_{0\mathrm{C}n}|$ are the tap changes from the initial state; $Q_{\mathrm{pv}0i}$ indicates the reactive power at the initial state and $\Delta Q_{\mathrm{pv}i}$ is the adjustment of the ith PV; and N_P, N_R, and N_C are the number of PVs, LTCs and VRs, and CBs, respectively. The weighting factors (W_P, W_R, and W_C) are added to exploit the reactive power capacity of PVs before mobilizing adjustment of the tap and, hence, to avoid unnecessary tap changes.

4.1.2. MINLP constraints The bus voltage is limited by (12), where V_LB and V_UB are the lower and upper bounds:

$$V_\mathrm{LB}\le V_j\le V_\mathrm{UB},\ j=1,\ldots,N-1 \tag{12}$$

The PV reactive power capability defined by (9) should be taken into account as in (13).

$$-Q_{\mathrm{pvmax}}-Q_{\mathrm{pv}0}\le\Delta Q_{\mathrm{pv}}\le Q_{\mathrm{pvmax}}-Q_{\mathrm{pv}0} \tag{13}$$

Finally, tap and CB positions are restricted by the respective bounds as shown in (14) and (15). Note that if the CB is single-step, then $S_{\mathrm{C\,min}}=0$ and $S_{\mathrm{C\,max}}=1$.

$$\mathrm{Tap}_{\mathrm{min}}\le\mathrm{Tap}\le\mathrm{Tap}_{\mathrm{max}} \tag{14}$$

$$S_{\mathrm{Cmin}}\le S_\mathrm{C}\le S_{\mathrm{Cmax}} \tag{15}$$

The above MINLP problem can be solved directly by using an optimization software such as the MATLAB Optimization Toolbox [21]. The solver *fmincon* in this toolbox can find the minimum of a function subject to nonlinear constraints. However, it treats all variables as continuous ones. Therefore, the discrete variables should be processed following the recommendation in [1].

Because the direct solving process faces some problems like computational time and local traps, we propose some approximations to convert the above general MINLP problem to a QP one and build a specific algorithm to solve it. A comparison between these two problems and the corresponding results will be carried out later in the Case Study section.

4.2. Formulation of a QP problem In this paper, a changing event is modeled by an adjusted power amount. The approach here is to minimize the sum of squares of all changing amounts at the same time. It turns out that the QP (16) can be applied.

$$\begin{cases}\underset{x}{\mathrm{Min}}\ \frac{1}{2}x^THx+f^Tx\\ \text{Subject to } Ax\le b;\ A_\mathrm{eq}x=b_\mathrm{eq};\ \mathrm{LB}\le x\le\mathrm{UB}\end{cases} \tag{16}$$

where $H, f, A, b, A_\mathrm{eq}, b_\mathrm{eq}$, LB, UB, and the variable x are defined in detail in the next subsections.

4.2.1. QP objective function From the power-based models in Section 3, the tap moving events ($\Delta\mathrm{Tap}_\mathrm{R}$ and ΔS_C) have been represented by power changes. Let us denote some parameters for the ease of expression: $\Delta Q_{\mathrm{R}k}$ is the fictitious reactive power resulting from moving the tap positions of an LTC or a VR at bus k in Fig. 2; $\Delta Q_{\mathrm{C}n}$ is the reactive power adjustment of the nth CB. The OF (11) is converted into a new one in (17) by noting that the square of $Q_{\mathrm{pv}0i}$ can be removed without any effect on the process of reaching the minimum point.

$$\underset{\Delta Q}{\mathrm{Min}}\left[W_\mathrm{P}'\sum_{i=1}^{N_\mathrm{P}}\left(\Delta Q_{\mathrm{pv}i}\right)^2+W_\mathrm{R}'\sum_{k=1}^{N_\mathrm{R}}\left(\Delta Q_{\mathrm{R}k}\right)^2+ W_\mathrm{C}'\sum_{j=1}^{N_\mathrm{C}}\left(\Delta Q_{\mathrm{C}n}\right)^2+W_\mathrm{P}'\sum_{i=1}^{N_\mathrm{P}}2Q_{\mathrm{pv}0i}\Delta Q_{\mathrm{pv}i}\right] \tag{17}$$

4.2.2. QP constraints The bus voltage in (12) can be defined as $V_j=V_{0j}+\Delta V_j$, where ΔV_j is approximated by (A14) in the Appendix. From that equation, the voltage limit is represented by (18), where the variable ΔQ_gen is a column vector of ΔQ_pv, ΔQ_R, and ΔQ_C.

$$\begin{bmatrix}K_{\mathrm{QV,red}}\\ -K_{\mathrm{QV,red}}\end{bmatrix}\Delta Q_\mathrm{gen}\le\begin{bmatrix}V_\mathrm{UB}+V_0\\ -V_\mathrm{LB}+V_0\end{bmatrix} \tag{18}$$

Other constraints are the same as in (13)–(15). The variables and matrices in (16) are assigned as follows:

- Variable: $x=\Delta Q_\mathrm{gen}$
- The Hessian matrix: $H=2I_\mathrm{w}$ where the off-diagonal elements of I_w are zero and the diagonal elements are the positive weighting factors W'_P, W'_C, and W'_R. It is obvious that H is a positive definite matrix. Therefore, the OF is strictly convex. Thus, the optimum obtained by solving the problem is global [21].
- The column vector f is defined as: $f=[0;\ 2W'_\mathrm{P}Q_{\mathrm{pv}0}]$.
- The inequality matrix A and the vector b are $A=[K_{\mathrm{QV,red}}, -K_{\mathrm{QV,red}}]^T$; $b=[V_\mathrm{UB}+V_0, -V_\mathrm{LB}+V_0]^T$.
- Bounds are defined by (13): $\mathrm{LB}=-Q_{\mathrm{pv\,max}}-Q_{\mathrm{pv}0}$, $\mathrm{UB}=Q_{\mathrm{pv\,max}}-Q_{\mathrm{pv}0}$.
- The equality constraint can be set based on a sharing mode among the inverters. However, this paper considers only a case without a sharing mode, i.e. A_eq and b_eq are empty.

The formulated QP optimization problem is still complicated to solve because the indirect variables Tap (for LTCs and VRs) and S_C (for CBs) are integer numbers while the reactive power variables representing PVs are continuous real numbers. Furthermore, the bounds (14) and (15) are implicit functions of the direct variable ΔQ_gen. The optimization problem is thus considered a mixed-integer QP.

4.3. Proposed algorithm To solve the above mixed-integer QP problem, the algorithm depicted in Fig. 3 is proposed.

The main idea of the algorithm is to convert the changing amounts of the discrete variables ($\Delta\mathrm{Tap}$, ΔS_C) into continuous variables (ΔQ_R, ΔQ_C) to formulate a strictly convex QP problem in Section 4.2, which can be well solved by methods like the active set or the interior point algorithm. For ease of description, this paper employs a built-in MATLAB solver named '*quadprog*' [21] to find a solution.

After solving the optimization problem with continuous variables, the constraints (14) and (15) are considered. The required tap position is estimated by substituting $\Delta Q_k=\Delta Q_{\mathrm{Rquad}}$ into (A5) in the Appendix to find the ratio t and (7) to find the position Tap, and a similar substitution of ΔQ_C in (8) to calculate S_C. Then, an appropriate Tap or S_C is selected so that it is an integer and satisfies (14) or (15), respectively. For instance, if the estimated Tap is not an integer, the rounded value is selected; if Tap is out of the tap range, the nearest limit is assigned to it. The algorithm stops if all voltages are inside the limits after the selection of discrete variables. Otherwise, the newly found optimum is set to be the initial value of the next iteration as shown in Fig. 3.

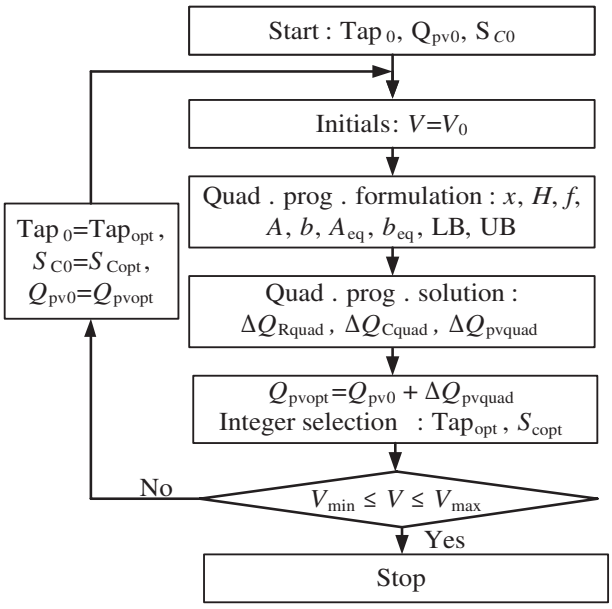

Fig. 3. Algorithm for mixed-integer quadratic programming

The final result is the optimal coordination ($\mathrm{Tap_{LTC}}$, $\mathrm{Tap_{VR}}$, S_C, Q_{pv}) that will be transmitted to the voltage regulating devices. The algorithm requires running the power flow program once for each iteration.

5. Optimal Compensation Factor in the Short Timescale

As introduced in Section 2.2, when a PV detects a change in the amount of ΔP_{pv}, the control system of that PV will calculate and supply an appropriate amount of ΔQ_{pv} through a factor – say a compensation factor K_{QP} – to maintain the connection voltage at the value prior to the change.

5.1. Compensation factor Assume that only the kth PV has fast reduction ΔP_{fpvk} and that this PV must be responsible for injecting reactive power ΔQ_{fpvk}. The changing voltage at bus i ($i = 1, \ldots, M = N-1$) is expressed by (19), where $K_{PV(ik)}$ and $K_{QV(ik)}$ indicate the elements at the ith row and kth column of matrices K_{PV} and K_{QV}, respectively. To maintain the voltage at the value immediately before the active power change, the voltage deviation should be minimized by solving (20).

$$\Delta V_i = K_{PV(ik)}\Delta P_{fpvk} + K_{QV(ik)}\Delta Q_{fpvk} \tag{19}$$

$$\mathrm{Min}\sum_{i=1}^{M}(K_{PV(ik)}\Delta P_{fpvk} + K_{QV(ik)}\Delta Q_{fpvk})^2 \tag{20}$$

Because ΔP_{fpvk} is already known, (20) is quadratic and minimized at the root of its derivative as shown in (21), where the compensation factor K_{QP} is determined by (22). Then, the necessary reactive power following the active power change is given by (23), which is the sum of the adjustment ΔQ_{fpvk} specified by (21) and the amount prior to the change Q_{pv0k} (the optimal VAr from the long timescale control). Obviously, Q_{fpvk} in (23) should be considered along with the condition (9).

$$\Delta Q_{fpvk} = K_{QP}\Delta P_{fpvk} \tag{21}$$

$$K_{QP} = -\sum_{i=1}^{M}(K_{PV(ik)}K_{QV(ik)})/\sum_{i=1}^{M}K_{QV(ik)}^2 \tag{22}$$

$$Q_{fpvk} = Q_{pv0k} + \Delta Q_{fpvk} \tag{23}$$

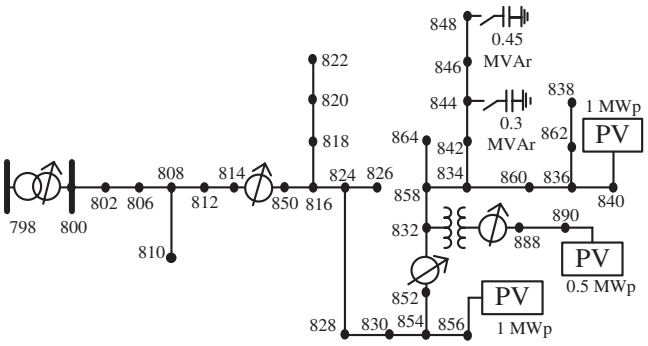

Fig. 4. Modified IEEE 34-bus feeder

5.2. Implementation and Effects The active power P^f_{pvk} is forecast periodically in the long timescale control. The change in the amount in the output (ΔP_{fpvk}) is determined by subtracting the power measured at the connection point by the forecast power, as given by (24):

$$\Delta P_{fpvk} = P_{pvk} - P^f_{pvk} \tag{24}$$

To prevent the inverter from overworking on adjusting the reactive power, a dead band of ΔP_{fpvk} can be set. For example, if $|\Delta P_{fpvk}| = 5\% P^f_{pvk}$, $\Delta Q_{fpvk} = 0$. This setting becomes useful when the PV active power is fairly stable on a sunny day and the changing effect on the voltage can be neglected.

The short timescale amount of reactive power in (23) was obtained with the assumption of changing the active power at only one PV while the others remain constant. In practical operation, the mutual interference of multiple PVs should be considered because more than one PV is likely to experience power fluctuation/intermittency simultaneously. Despite that fact, the influence of the proposed short timescale control is expected to be positive.

6. Case Study

The power-based models and the proposed algorithm can work well in distribution systems including multiple feeders. However, to verify the method and illustrate its effectiveness, a single feeder with some regulating devices is selected.

6.1. Test system The test system in Fig. 4 is a modification of the IEEE 34-bus system [22]. The original unbalanced system was modified to a balanced one for a straightforward demonstration. The test system contains two high-impedance transformers and some long lines (806–814, 818–820, 856–854–852, and 888–890), which results in serious voltage drops along the feeder. Hence, one LTC and three VRs were installed as in Ref. [23]. In addition, this paper also considers two ON/OFF CBs operated by the utility company and three PVs with parameters shown in Fig. 4. The maximum load of the system is $1.769 + \mathrm{j}1.044$ megavar (MVAr). The statutory limit of the bus voltages is [0.95 p.u., 1.05 p.u.] except at the output terminals of LTC and VRs where the voltage can range from 0.9 to 1.1 p.u.

6.2. Verification For the sake of verifying the proposed method, only three devices were considered for adjustment (marked as 'var'), while others were at fixed settings to assist the voltage profile as provided in Table I. The main purpose of limiting the number of devices is to reduce the number of combinations to be assessed for finding the true global optimum. If each combination is considered as one point in the search space, a reliable optimum point can be obtained by assessing all possible

Table I. Settings for verification

Bus	PV ratings (MW)	P_{pv} (MW)	Q_{pv} (MVAr)	Tap	CB
798	—	—	—	0	—
814	—	—	—	0	—
852	—	—	—	var	—
888	—	—	—	9	—
844	—	—	—	—	OFF
848	—	—	—	—	var
840	1	0.5	var	—	—
856	1	1	0	—	—
890	0.5	0	0	—	—

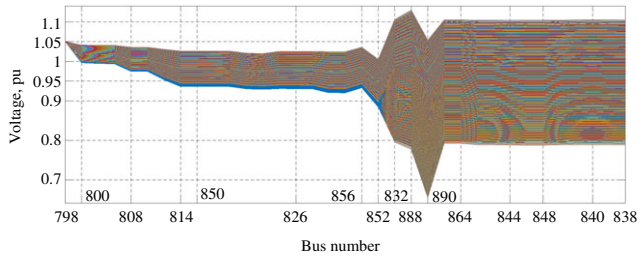

Fig. 5. Voltage profiles of all possibly coordinating combinations

combinations of tap positions, CB switching states, and PV power. This point will be used as a reference to examine the accuracy of the proposed method in the long timescale control.

In the verification, load was assumed at the maximum demand, and the voltage at bus 798 was fixed at $V_{798} = 1.05$ p.u. PV840 was generating 0.5 MW at $\cos\varphi \geq 0.85$, as specified by (9). Hence, the corresponding VAr limitation was 0.31 MVAr.

6.2.1. True global optimum The reactive power of PV840 was changed discretely in steps of 0.01 MVAr (about 1% of the PV rating). Thus, there were 63 values ranging from −0.31 to +0.31 MVAr. When combined with 33 positions (including tap zero) of VR852 and two states of close/open (ON/OFF) of CB848, the number of points to be examined is $63 \times 33 \times 2 = 4158$.

A combination of [$\text{Tap}_{\text{VR852}}$, S_{C848}, Q_{pv840}] is considered as the global optimum if it minimizes the OF (11) and all bus voltages are inside the specified limits. The weighting factors were selected as $W_{\text{P}} = 1$, $W_{\text{R}} = 100$, and $W_{\text{C}} = 1$ so that the optimization solver in the next subsections would tend to change the PV power and CB switching state rather than adjusting the tap positions. The initial coordination was assumed as [$\text{Tap}_{\text{VR852}} = 0$, $S_{\text{C848}} = 0$, $Q_{\text{pv840}} = 0$]. After going through all combinations, the system voltage profiles are as shown in Fig. 5. The true global optimum was found as OF = 1601.1; $\text{Tap}_{\text{VR852}} = 4$; $S_{\text{C848}} = 1$; and $Q_{\text{pv840}} = 0.28$ MVAr. With this optimum, bus 890 experienced the lowest voltage of the downstream feeder at 0.95 p.u. It is informative to report that the examination performed on the DELL Inspiron Core i7 4500U consumed about 33 min to examine all points, which is too long for real-time control.

6.2.2. Optimal solution obtained by using the MINLP solver The verification here employed the sequential QP (SQP) algorithm to find the minimum of the function (11) subject to the nonlinear constraints (12)–(15). At the initial step, the VR852 was at the $\text{Tap}_{\text{VR8520}} = 0$; the CB is OFF ($S_{\text{C0848}} = 0$); and $Q_{\text{pv0840}} = 0$. Table II presents statistics describing the calculations in each iteration. In the last iteration, the SQP stopped at [$\text{Tap}_{\text{VR852}} = 3.577$, $S_{\text{C848}} = 1$, $Q_{\text{pv840}} = 0.31$ MVAr]. After the tap rounding process, all constraints were still satisfied, and the final solution was accepted as [$\text{Tap}_{\text{VR852}} = 4$, $S_{\text{C848}} = 1$, $Q_{\text{pv840}} = 0.31$ MVAr] when

Table II. MINLP iterative display

Iter.	F-count	$f(x)$	Feasibility	Optimality
0	4	0	1.174e − 01	1.490e − 06
1	19	0.393	1.151e − 01	1.247e + 01
2	23	1021.247	3.229e − 03	6.387e + 02
3	27	1280.477	1.160e − 06	1.850e + 02
4	31	1280.575	1.694e − 12	6.368e − 03
5	35	1280.575	3.331e − 16	3.331e − 16

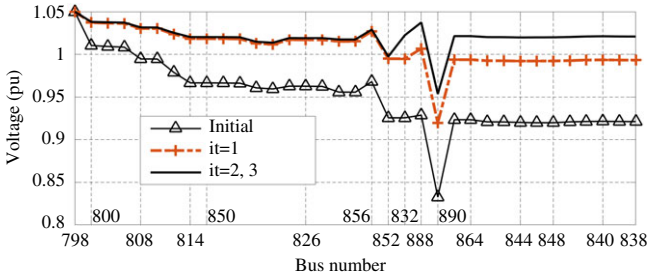

Fig. 6. Voltage profile when running the proposed algorithm

both changes in the optimality, which is a measure of how close a point x is to the optimal point, and the feasibility, which represents the maximum constraint violation, were less than a predetermined valued of 10^{-6}. There were 35 points where the evaluations of the OF and constraints were done. This also means the solver needed at least 36 power flow running times (including one running time for checking the final solution). To converge and reach the local optimum point, the above MINLP solver consumed about 31 s when running on the same computer as the one in Section 6.2.1. Although the obtained point in this case is close to the global optimum in Section 6.2.1, the above MINLP generally cannot guarantee that it is the global one.

6.2.3. Optimal solution obtained by using the proposed method From the same initial point used by the MINLP solver above, the algorithm was started, and it stopped after three iterations at the final solution: [$\text{Tap}_{\text{VR852}} = 4$, $S_{\text{C848}} = 1$, $Q_{\text{pv840}} = 0.31$ MVAr]. There were four times running power flow, including three times for three iterations and another one for initializing the algorithm, as required by the program. The absolute time to reach the final solution was about 3.2 s.

The system voltage after each iteration is plotted in Fig. 6, where the plotting range was limited to [0.8 p.u., 1.05 p.u.], which was smaller than the range in Fig. 5 for better illustration. Note that bus 888 experienced higher voltages than buses 852 and 832 after the first iteration because the VR888 had been fixed at Tap = 9, as shown in Table I. The first iteration required $Q_{\text{pv840}} = 0.31$ MVAr and changed the status of the CB848 from OFF to ON; hence the algorithm fixed it at the state of 'switching ON' for all iterations onwards and restarted with only two variables ΔQ_{VR852} and ΔQ_{pv840}. In the second iteration, the initial point was [$\text{Tap}_{\text{VR852}} = 0$, $Q_{\text{pv840}} = 0.31$ MVAr]. After rounding $\text{Tap}_{\text{VR852}}$ from 3.85 to 4 at this iteration, the algorithm restarted and checked all bus voltages inside the limits and stopped. This explains why the voltage profiles of the second and third iterations were identical. The similarity between them also proves that Assumption 3 in the Appendix is acceptable, and that the power-based models of LTCs and VRs can be approximated by using the initial voltage as assumed after (A12) in the Appendix.

The final solution [$\text{Tap}_{\text{VR852}} = 4$, $S_{\text{C848}} = 1$, $Q_{\text{pv840}} = 0.31$ MVAr] obtained from the proposed algorithm is the same as the one found by the MINLP solver and close to the true global optimum [$\text{Tap}_{\text{VR852}} = 4$, $S_{\text{C848}} = 1$, $Q_{\text{pv840}} = 0.28$ MVAr].

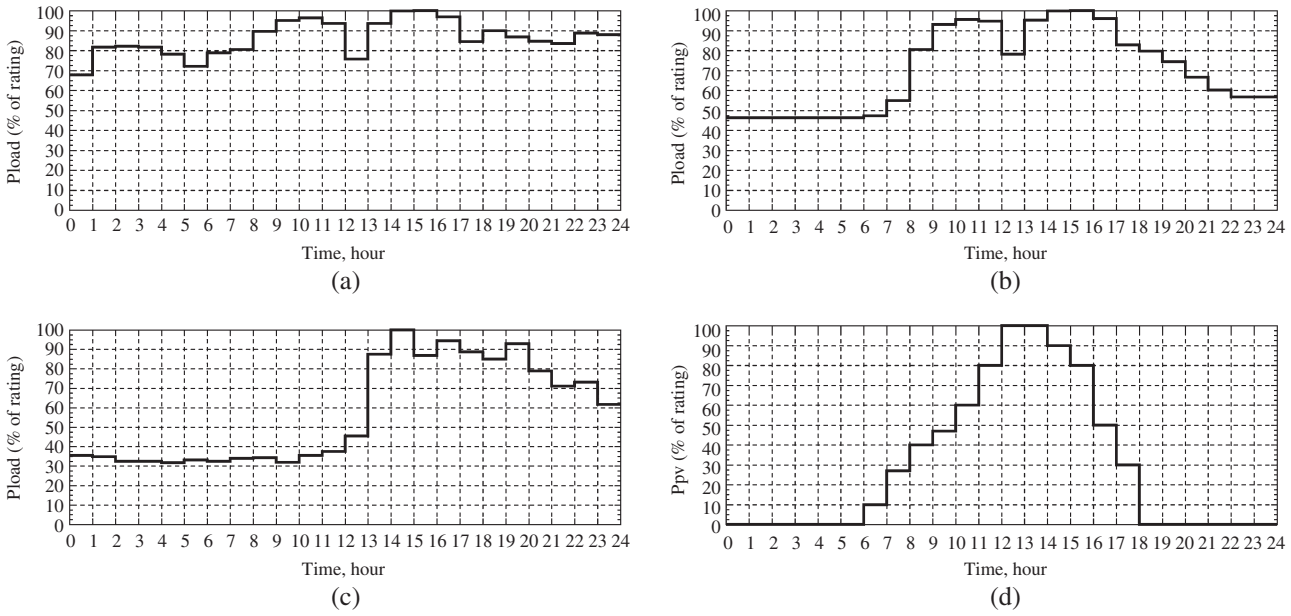

Fig. 7. Forecast load demand and PV generation. (a) Industrial load: (822, 890, 844, 846, 860); $S_{\text{load max}} \geq 0.1$ MVA. (b) Commercial load: (806, 830, 836, 840), $0.05 < S_{\text{load max}} < 0.1$ MVA. (c) Residential load ($S_{\text{load max}} \leq 0.05$ MVA) (d) PVs (840, 856, 890)

The error is only because of the tap rounding and the selected step of 0.02 MVAr when examining all feasible combinations. In the proposed method, reactive power of PV840 was exploited first, and then tap movement was utilized. The QP originally required $\text{Tap}_{\text{VR852}} = 3.85$ at $Q_{\text{pv840}} = 0.31$ MVAr. After rounding the tap up to 4, the requirement of 0.31 MVAr became a bit more than the minimum value at 0.28 MVAr in the true optimum.

Compared to direct MINLP solver, the proposed QP algorithm is more advantageous. First, the computational time was reduced significantly (about 10 times), and this advantage is supposed to be more significant when the size of the tested system is larger. Second, while the MINLP solver could fall into local optimum traps, the proposed method is guaranteed to reach a near-global optimum. Therefore, in the next section we illustrate the effectiveness of the proposed method on the background of the conventional control technique.

When applying to a system with more regulating devices, the error may also be due to the approximations to linearize the optimization problem. On the other hand, a reward for taking the error is the fast execution and the robustness of the proposed algorithm.

In the above verification, the rounding of the single-step CB's switching states had a great impact on the convergence of both the MINLP and QP algorithms. This is because the involved capacitor was relatively large compared to the total reactive power load (0.45 MVAr/1.044 MVAr = 43.10%). Therefore, after rounding the switching state of the CB, it should be eliminated from the variable set. For a smaller CB or a multistep CB, the elimination may be unnecessary.

6.3. More voltage regulating devices

6.3.1. Long timescale control The system was tested for the whole-day operation and considering all the devices marked in Fig. 4. The forecast load profiles and PV active power in Fig. 7 were referred to the typical load profile of the Provincial Electricity Authority (PEA), Thailand. The proposed algorithm in the long timescale layer was applied from 6 am to 6 pm when the PV generated active power. At night, the system was operated as usual with the conventional technique. For the ease of demonstrating the method, loads and PV generations were plateaus during each hour step. If more accurate control is targeted, each hour can be divided into smaller parts, for example, four 15-min periods as introduced Section 2.1. The proposed method was compared with the conventional control technique as follows:

Table III. Requirement of voltage limits

Bus	Conventional method	Optimal method (p.u.)
814, 890	120 ± 1 V	$1 \pm 1/120$
852	122 ± 1 V	$1.0167 \pm 1/120$
838	124 ± 1 V	$1.0333 \pm 1/120$
800, 850, 816, 818, 832, 888	[0.90, 1.10] p.u.	[0.90, 1.10]
Others	[0.95, 1.05] p.u.	[0.95, 1.05]

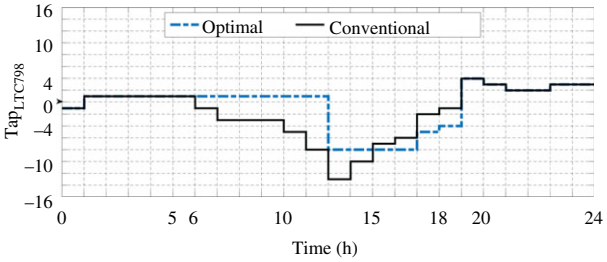

Fig. 8. LTC798 tap positions over 24 h

Conventional control technique: When considering the daily operation, PVs were fixed at the unity power factor and the CBs were switched ON for the whole day because its main function is to support reactive power. The response of the conventional control at the beginning of each hour step was simulated by running power flow to estimate the bus voltages. Each LTC or VR was operated at a particular regulation point along with a specified voltage setpoint as shown in Table III. More settings are presented in Table AI in the Appendix.

Figures 8–11 record the changing operation of LTC and VRs over 24 h. The results show that they are required to move their taps quite frequently from 5:00 to 20:00 when fluctuation of large loads (industrial and commercial) and PV generation influenced the system.

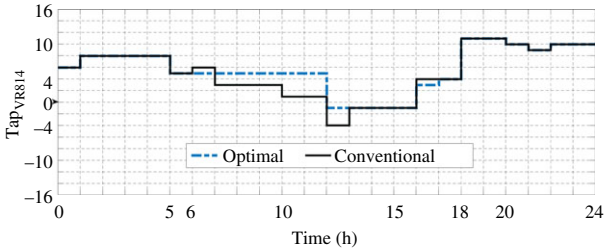

Fig. 9. VR814 tap positions over 24 h

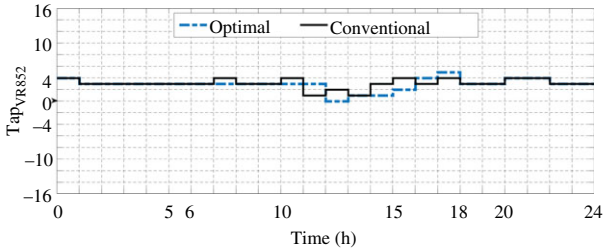

Fig. 10. VR852 tap positions over 24 h

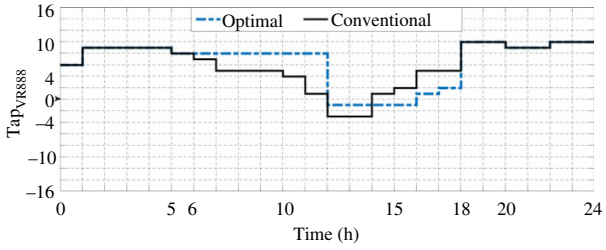

Fig. 11. VR888 tap positions over 24 h

Proposed control technique: It is worth noting that the LTC is supplied by the slack bus 798. Thus, the additionally injected power source ($\Delta P_{798} + \mathrm{j}\Delta Q_{798}$) is unnecessary in formulating the optimization problem, i.e. $K_{\mathrm{P798-800}} = 0$ and $K_{\mathrm{Q798-800}} = 0$.

For further comparison in this section, the proposed control was performed under the same condition as used by the conventional technique. This condition is summarized in Table III, where the voltage limits of four regulation points (814, 852, 838, 890) were picked up from Table AI in the Appendix: $V_{\mathrm{limit}} = V_{\mathrm{set}} \pm 0.5 \times$ bandwidth. A wider range of [0.9–1 p.u.] was applied to the output of LTC and VRs and no-load buses 816 and 818 behind the VR814. This is acceptable because the line 818–820 is extremely long, about 9 miles.

At the beginning of each hour, the central controller determined one optimal coordination, which would be expected to keep the voltage within the designated limits. The optimal tap positions are also recorded in Figs 8–11 for comparison.

The number of tap changing times over 24 h was significantly reduced when using the proposed control. Table IV shows that the average reduction was estimated at about 36.46%. These numbers of operating times of LTC and VRs would be expected to be smaller if the voltage limits in Table III were extended. This is reasonable because the purpose of setting a strict V_{set} along with a narrow bandwidth is to create a conservative range to compensate the controlling error and to avoid overworking the tap mover in the conventional control. Under a reliable calculation of the optimal control, the voltage limit can be confidently extended to a wider range.

Using reactive power of PVs played a very important role in reducing the number of tap operations per day. If the '+' sign indicates generating power and the '−' sign is for absorbing

Table IV. Number of operating times per day

Scheme	LTC798	VR814	VR852	VR888
Conventional	15	12	14	13
Optimal	8	9	9	8
Reduction (%)	46.67	25	35.71	38.46

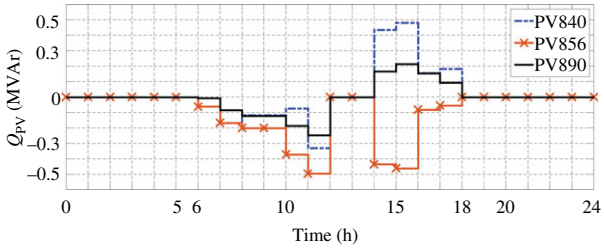

Fig. 12. Reactive power of PVs over 24 h (optimal control)

Table V. Compensation factors from 14:00 to 15:00

PV buses	P^f_{pv} (MW)	$Q_{\mathrm{pv(opt)}}$ (MVAr)	K_{QP}
PV840	0.9	0.436	−0.90
PV856	0.9	−0.436	−0.71
PV890	0.45	0.166	−0.83

power, Fig. 12 shows that PVs were asked for supporting reactive power throughout the day except during the time from 12:00 to 14:00 when all PVs generated their peak MW power ($\mathrm{MW_p}$). The advantage is that the power factor was never less than 0.85, thereby always satisfying the utility requirement.

Regarding the CBs, both were required to be connected to the system almost all day long like the requirement in the conventional control. There was only a 1-h step from 12:00 to 13:00 when CB848 was switched OFF.

6.3.2. Short timescale control In the simulation, an arbitrary period was selected, e.g. from 14:00 to 15:00, for illustrating the operation of the short timescale control. During the selected time, the forecast load was constant at 100% of the maximum demand and the PV was forecast at 90% of the rated MW, as shown in Fig. 7. The settings of LTC, VRs, and the PV reactive power had been optimized by the long timescale control: $\mathrm{Tap_{LTC}} = -8$, $\mathrm{Tap_{VR814}} = -1$, $\mathrm{Tap_{VR852}} = 1$, $\mathrm{Tap_{VR888}} = -1$, $Q_{\mathrm{pv840}} = 0.436\,\mathrm{MVAr}$, $Q_{\mathrm{pv856}} = -0.436\,\mathrm{MVAr}$, and $Q_{\mathrm{pv890}} = 0.166\,\mathrm{MVAr}$. Compensation factors for the interested hour were computed by using (22) and are presented in Table V.

Simulation results showed that the short timescale control successfully held the voltage profile within [0.95 p.u., 1.05 p.u.] if only one PV lost its currently generating active power, as shown in Fig. 13. Such a reduced amount occurred in a very short time, which was smaller than the delay time of the LTC or the VRs. Therefore, the tap changers did not respond to the voltage change.

In the second test, all three PVs lost their active power completely and simultaneously. They compensated the MW reduction by injecting the VAr capability at their ratings: $Q_{\mathrm{pv840}} = 1\,\mathrm{MVAr}$, $Q_{\mathrm{pv856}} = 1\,\mathrm{MVAr}$, and $Q_{\mathrm{pv890}} = 0.5\,\mathrm{MVAr}$. All buses further than bus 856 (compared to the substation at bus 798) experienced voltages lower than 0.95 p.u., as shown in Fig. 13.

The above unsuccessful short timescale control can be explained by the high *R/X* ratio in distribution systems. This ratio makes the voltage drop, which is caused by the flow of active power, hard to be completely compensated by pumping reactive power from just some points. Solutions to this might be limiting the installed

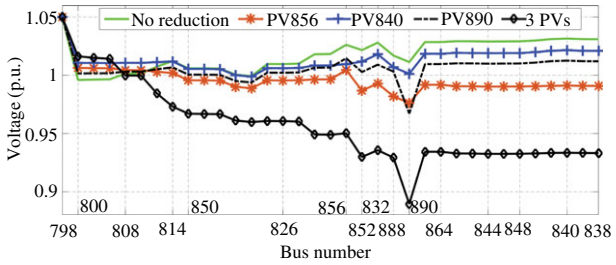

Fig. 13. Voltage profile when PVs have lost all active power

capacity of PVs and installing a controllable energy storage at the PV terminal. Furthermore, the vulnerability of the lowest voltage bus can be reduced by launching the optimization in the long timescale control at a higher V_{LB}, for example, $V_{\mathrm{LB}} = 0.96$ p.u., to broaden the conservative range under the normal condition. So, bus voltages are expected to be higher than 0.95 p.u. under the condition of sudden MW reduction.

7. Conclusion

In this paper,we proposed a very effective method for optimally coordinating voltage regulating devices with PVs in distribution systems and for reducing the number of tap changes during daily operation. The power-based model is the key factor for linearizing the system equation and formulating a mixed-integer QP problem. Application of the proposed method to a case study proved that the voltage profile along the feeder could be controlled successfully by the two-layer structure, by reducing the number of changing tap per day. Besides generating the near-global optimum, other prominent features of the proposed algorithm are the robustness and fast execution when working with multiple variables.

The two-layer structure can also deal with fast active power reduction. Although it can handle successfully the voltage profile by using the proposed compensation factor in some cases, some buses still violate the voltage lower limit when the MW reduction occurs simultaneously at more than one PV. The limited capability of the short timescale control in this paper partly explains why the penetration level of solar PVs should be limited unless PVs are equipped with battery energy storage systems or the lower bound in the long timescale control is selected at a higher level.

Appendix

Assumptions

Assumption 1 There are N buses, including one slack bus and other four bus groups: N_{R} LTCs and VRs, N_{C} CBs, and N_{P} PVs, and the remaining buses (N_{L}), without any of the above regulating devices. Note that a model of each LTC or VR occupies two buses, as shown in Fig. 2(b).

Assumption 2 No two LTCs or VRs are located on two neighboring lines, and each bus has one CB or PV. This assumption allows each bus to be connected to variables from only one regulating device, thereby helping us to clarify the analysis later. In practice, two VRs or LTCs may be routed from the same bus (bus h in Fig. 2(a)), and a CB is sometimes located at the substation bus for power factor correction. This assumption is still acceptable and it will be elaborated at the end of the Section Approximations of system equations.

Assumption 3 At an iteration, the initial point is not far from the optimum, so the new tap position is near the initial position, i.e. Δt is very small, and terms with $(\Delta t)^2$ can be neglected in an algebraic summation. The acceptability of this assumption has been proved at the end of the second paragraph of Section 6.2.3.

Approximations of system equations All approximations and equations described here are for representing the amount of voltage change due to the changing reactive power as a result of moving the taps, switching CBs, and adjusting reactive power of PVs. This representation was used for the voltage constraint (18) in Section 4.2.2.

The approximation starts with the system equations of a balanced three-phase power system represented in the form of power injection, which is an algebraic sum of all power flowing in and out of a bus. These equations imply that there are at the maximum two power expressions (active and reactive power) at any bus. The relationship between the changes of power and voltage can be given by (A1). Provided that the coefficient matrix J (the so-called Jacobian in this case) evaluated at V_0, which is the system voltage before getting changed by controlling voltage, is well conditioned, its inversion, denoted by K, is defined by (A2):

$$\begin{bmatrix} \Delta P \\ \Delta Q \end{bmatrix} = \begin{bmatrix} J_{\mathrm{P}\delta} & J_{\mathrm{PV}} \\ J_{\mathrm{Q}\delta} & J_{\mathrm{QV}} \end{bmatrix} \begin{bmatrix} \Delta \delta \\ \Delta V \end{bmatrix} \tag{A1}$$

$$K = J^{-1} = \begin{bmatrix} J_{\mathrm{P}\delta} & J_{\mathrm{PV}} \\ J_{\mathrm{Q}\delta} & J_{\mathrm{QV}} \end{bmatrix}^{-1} = \begin{bmatrix} K_{\mathrm{P}\delta} & K_{\mathrm{Q}\delta} \\ K_{\mathrm{PV}} & K_{\mathrm{QV}} \end{bmatrix} \tag{A2}$$

Before adjusting the power and tap positions, the initial voltage at bus j ($j = 1, \ldots, N-1$) is V_{0j}, and the voltage after that is V_j. The change will be $\Delta V_j = V_j - V_{0j}$. The vector ΔV in (A1) involving ΔV_j can be computed by (A3):

$$\Delta V = \begin{bmatrix} K_{\mathrm{PV}} & K_{\mathrm{QV}} \end{bmatrix} \begin{bmatrix} \Delta P & \Delta Q \end{bmatrix}^T \tag{A3}$$

In (A3), the coefficient matrix $[K_{\mathrm{PV}}\ K_{\mathrm{QV}}]$ is of order $(N-1) \times 2(N-1)$, while the lengths of the variable vector $[\Delta P\ \Delta Q]^T$ and the voltage deviation vector are $2(N-1)$ and $(N-1)$, respectively. It is to be noted that there are many buses with zero ΔP and/or ΔQ. The following paragraphs will represent (A3) by only $\Delta Q_{\mathrm{gen}} = \{\Delta Q_{\mathrm{pv}}, \Delta Q_{\mathrm{R}}, \Delta Q_{\mathrm{C}}\}$, which relates directly to the voltage regulating devices, by using the following elimination process:

Regarding the load buses, if bus j is an element of the set N_{L}, the power injection bus j remains constant. Hence, the corresponding columns (indexed by $j-1$) in K_{PV} and K_{QV} will be eliminated, and variables $(\Delta P_{j-1}, \Delta Q_{j-1})$ will also be cut out.

When it comes to buses with LTCs or VRs, the imaginary and real parts of (5) and (6), which are the fictitious power sources in Section 3, can be separated and written as (A4)–(A11) with the assistance of Assumption 3, which allows us to neglect $(\Delta t)^2$ in the summation:

$$\Delta Q_k = \Delta t |V_k||V_h|(g \sin \Delta\delta_{kh} - b \cos \Delta\delta_{kh}) \tag{A4}$$

$$\Delta t = \Delta Q_k / [\,|V_k||V_h|(g \sin \Delta\delta_{kh} - b \cos \Delta\delta_{kh})\,] \tag{A5}$$

$$\Delta P_k = K_{\mathrm{P}kk} \Delta Q_k \tag{A6}$$

$$K_{\mathrm{P}kk} = \frac{g \cos \Delta\delta_{kh} + b \sin \Delta\delta_{kh}}{g \sin \Delta\delta_{kh} - b \cos \Delta\delta_{kh}} \tag{A7}$$

$$\Delta P_h = K_{\mathrm{P}hk} \Delta Q_k \tag{A8}$$

$$K_{\mathrm{P}hk} = \frac{g \cos \Delta\delta_{hk}}{g \sin \Delta\delta_{kh} - b \cos \Delta\delta_{kh}} - \frac{2tg|V_h|}{|V_k|(g \sin \Delta\delta_{kh} - b \cos \Delta\delta_{kh})} + \frac{b \sin \Delta\delta_{hk}}{g \sin \Delta\delta_{kh} - b \cos \Delta\delta_{kh}} \tag{A9}$$

Table AI. Settings in the conventional scheme

Parameters	LTC798	VR814	VR852	VR888
Regulation point	814	852	838	890
PT ratio	120	120	120	20
CT's primary rating (A)	100	100	100	100
Z_{set} (V)	$17.91+\text{j}13.27$	$16.31+\text{j}7.90$	$3.19+\text{j}1.62$	$11.20+\text{j}8.33$
Bandwidth (V)	2	2	2	2
V_{set} (V)	120	122	124	120
Delay time (s)	90	60	40	30
CBs: switched ON for the whole day; PVs: unity power factor.				

PT: potential transformer; CT: current transformer.

$$\Delta Q_h = K_{Qhk}\,\Delta Q_k \tag{A10}$$

$$K_{Qhk} = \frac{g\sin\Delta\delta_{hk}}{g\sin\Delta\delta_{kh} - b\cos\Delta\delta_{kh}} - \frac{b\cos\Delta\delta_{hk}}{g\sin\Delta\delta_{kh} - b\cos\Delta\delta_{kh}} + \frac{b|V_h|2t}{|V_k|(g\sin\Delta\delta_{kh} - b\cos\Delta\delta_{kh})} \tag{A11}$$

In (A4)–(A11), there are $4N_{\text{R}}$ variables relating to LTCs and VRs, but $3N_{\text{R}}$ of them (ΔP_k, ΔP_h, and ΔQ_h) are represented by N_{R} variables ΔQ_k. These $3N_{\text{R}}$ variables in $[\Delta P,\ \Delta Q]^T$ are thus eliminated and the corresponding columns in K_{PV} and K_{QV} are removed. For example, the columns relevant to an LTC at branch $h-k$ are the columns $h-1$ and $k-1$ in K_{PV} for ΔP_h and ΔP_k, respectively; columns $h-1$ and $k-1$ in K_{QV} for ΔQ_h and ΔQ_k, respectively; columns $h-1$ and $k-1$ in K_{PV} and $h-1$ in K_{QV} are removed from $[K_{\text{PV}}\ K_{\text{QV}}]$, whereas column $k-1$ in K_{QV} is updated as shown in (A12) where $i=1,\ \ldots,\ N-1$.

$$[K_{\text{QV}}]^{\text{new}}_{i\times(k-1)} = [K_{\text{QV}}]^{\text{old}}_{i\times(k-1)} + K_{\text{P}hk}[K_{\text{PV}}]^{\text{old}}_{i\times(h-1)} + K_{\text{P}kk}[K_{\text{PV}}]^{\text{old}}_{i\times(k-1)} + K_{Qhk}[K_{\text{QV}}]^{\text{old}}_{i\times(h-1)} \tag{A12}$$

Although V_h and V_k are not known yet (hence the coefficient factors $K_{\text{P}kk}$, $K_{\text{P}hk}$, and K_{Qhk} cannot be specified), the voltage ratio $|V_h|/|V_k|$ and angles (δ_h, δ_k) after regulating voltage can be approximated by using the voltages at the initial state. This approximation is acceptable in an iteration technique because the next initial state is closer to the final solution than the initial state of the previous iteration. This was illustrated and explained in the second paragraph of Section 6.2.3.

Unlike the LTC and VR buses, each bus with a PV or a CB goes with one variable of changing reactive power while the active power changes are zero. The columns relevant to the active power changes of PVs and CBs are cut out of (A3).

Finally, the matrix K_{PV} is completely eliminated and the $(N_{\text{R}}+N_{\text{L}})$ columns of K_{QV} are removed. The element number of $[\Delta P\ \ \Delta Q]^T$ is reduced to $N_{\text{UNK}}=(N_{\text{R}}+N_{\text{C}}+N_{\text{P}})$, which is the result of subtracting $2(N-1)$ variables by $(3N_{\text{R}}+2N_{\text{L}}+N_{\text{C}}+N_{\text{P}})$ variables because Assumptions 1 and 2 provide the linkage (A13) among the four bus groups.

$$N-1 = 2N_{\text{R}}+N_{\text{C}}+N_{\text{P}}+N_{\text{L}} \tag{A13}$$

The new coefficient matrix now is the reduced K_{QV}, denoted by $K_{\text{QV,red}}$, and is of order $(N-1)\times(N_{\text{R}}+N_{\text{C}}+N_{\text{P}})$. After all, the voltage changing vector after adjustment is given by (A14). This equation has been used for expressing the voltage constraint (18) in Section 4.2.2.

$$\Delta V = K_{\text{QV,red}}\,\Delta Q_{\text{gen}} \tag{A14}$$

According to Assumption 2, each bus has variables coming from only one control device directly connected to that bus. Such an assumption helps in making the definition of ΔQ_{gen} more straightforward. Rejection of this assumption does not change the number of variables in the vector ΔQ_{gen}, but additionally intermediate equations should be formulated. For instance, if a CB is connected to the substation bus of the LTC (bus k in Fig. 2), there will be two types of ΔQ_{gen} at bus k (ΔQ_{Ck} and $\Delta Q_{\text{LTC}\,k}$) and $\Delta Q_{\text{gen}\,k}$ represents the sum of these two variables: $\Delta Q_{\text{gen}\,k}=\Delta Q_{Ck}+\Delta Q_{\text{LTC}\,k}$. When separating ΔQ_{Ck} from $\Delta Q_{\text{gen}\,k}$, all rows in $K_{\text{QV,red}}$ are retained and a new column is added to it, and the vector variable ΔQ_{gen} will have a new element ΔQ_{Ck}.

Settings in the conventional control Settings of LTC and VRs in Table AI were performed with some suggestions in [22,23], but some changes had been made to adapt the system with the introduction of the LTC at the source bus. Particularly, the impedance Z_{set} of the LDC circuit of the LTC and VRs was calculated based on the following scenario:

- All PVs are disconnected.
- All CBs are OFF.
- All loads are at the maximum demand.
- Power flow is used to compute the equivalent line impedance as $R_{\text{line}}+\text{j}X_{\text{line}}=(VR_{\text{output}}-V_{\text{reg. point}})/I_{\text{line}}$

Acknowledgments

This work was partly supported by Rachadapisek Sompote Fund for Postdoctoral Fellowship, Chulalongkorn University, and also by the Ratchadapisek Sompoch Endowment Fund (2016), Chulalongkorn University (CU-59-051-EN).

The authors would like to thank the Department of Electrical Engineering, Faculty of Engineering, Chulalongkorn University, and the AUN/SEED-Net Project of JICA for the important support for collaboration with the Advanced Collaborative Research Organization for Smart Society (ACROSS), Waseda University, Japan, under the Short-Term Research Program in Japan (SRJP) of the year 2016.

References

(1) Kulmala A, Repo S, Järventausta P. Coordinated voltage control in distribution networks including several distributed energy resources. *IEEE Transactions on Smart Grid* 2014; **5**(4):2010–2020.
(2) Ranamuka D, Agalgaonkar AP, Muttaqi KM. Online voltage control in distribution systems with multiple voltage regulating devices. *IEEE Transactions on Sustainable Energy* 2014; **5**(2):617–628.
(3) Salih SN, Chen P. On coordinated control of OLTC and reactive power compensation for voltage regulation in distribution systems with wind power. *IEEE Transactions on Power Systems* 2015; **31**(5):4026–4035.
(4) Kikusato H, Takahashi N, Yoshinaga J, Yu F, Hayashi Y, Kusagawa S, Motegi N. Method for rapidly determining line drop compensator

parameters of low-voltage regulator using classifiers. *IEEJ Transactions on Power and Energy* 2015; **135**(7):446–453.
(5) Yoshizawa S, Yamamoto Y, Hayashi Y, Sasaki S, Shigeto T, Nomura H. Dynamic updating method of optimal control parameters of multiple advanced SVRs in a single feeder. *IEEJ Transactions on Power and Energy* 2015; **135**(9):550–558.
(6) Kawano S, Ohkubo S, Yoshizawa S, Fujimoto Y, Hayashi Y. OLTC and multiple SVRs in distribution system by using database. *Proceedings of the 5th International Youth Conference on Energy* (*IYCE*), 2015.
(7) Baerthlein E-M, Hartung M, Panosyan A. Variable voltage set point control of tap changers in distribution grids. *Proceedings of the IEEE PES Innovative Smart Grid Technologies Europe* (*ISGT Europe*), 2014.
(8) Baerthlein E-M, Hartung M, Panosyan A, Witzmann R. Variable bandwidth control of tap changers in distribution grids. *Proceedings of IEEE PES Innovative Smart Grid Technologies Europe* (*ISGT Aisa*), 2015.
(9) Yokoyama A, Akagi H, Hayashi Y, Ogimoto K, Ishii H. A national project on optimal control and demonstration of the Japanese smart grid for massive integration of photovoltaic systems. *Proceedings of IEEE PES Innovative Smart Grid Technologies Europe* (*ISGT Europe*), 2012.
(10) Farivar M, Clarke CR, Low SH, Chandy KM. Inverter VAR control for distribution systems with renewables. *Proceedings of IEEE International Conference on Smart Grid Communications* (*SmartGridComm*), 2011.
(11) Paaso EA, Liao Y, Cramer AM. Dual-layer voltage and VAR control approach with active participation from distributed solar generations. *Electric Power Components and Systems* 2015; **43**(8–10):854–865.
(12) Ahmadi H, Marti JR, Dommel HW. A framework for Volt-VAR optimization in distribution systems. *IEEE Transactions on Smart Grid* 2015; **6**(3):1473–1483.
(13) Miyamoto Y, Hayashi Y. Evaluation of improved generation efficiency through residential PV voltage control of a clustered residential grid-interconnected PV. *Proceedings of IEEE PES Innovative Smart Grid Technologies Conference Europe* (*ISGT Europe*), 2010.
(14) Kersting WH. *Distribution System Modeling and Analysis*. 2 ed. CRC Press; 2007.
(15) Schneider KP, Fuller JC, Chassin D. Evaluating conservation voltage reduction: an application of GridLAB-D: an open source software package. *Proceedings of IEEE PES General Meeting*, 2011.
(16) Roytelman I, Ganesan V. Modeling of local controllers in distribution network applications. *IEEE Transactions on Power Delivery* 2000; **15**(4):1232–1237.
(17) Dzafic I, Mohapatra P, Neisius HT. Modeling of automatic local controllers in three phase load flow calculation. *Proceedings of IEEE PES Innovative Smart Grid Technologies* (*ISGT*), 2011.
(18) Dzafic I, Jabr RA, Halilovic E, Pal BC. A sensitivity approach to model local voltage controllers in distribution networks. *IEEE Transactions on Power Systems* 2014; **29**(3):1419–1428.
(19) Verboomen J, Van Hertem D, Schavemaker PH, Kling WL, Belmans R. Phase shifting transformers: principles and applications. *Proceedings of International Conference on Future Power Systems*, 2005.
(20) Hongbo S, Nikovski D, Ohno T, Takano T, Kojima Y. Hybrid three-phase load flow method for ungrounded distribution systems. *Proceedings of IEEE PES International Conference and Exhibition on Innovative Smart Grid Technologies* (*ISGT Europe*), 2012.
(21) MathWorks. *MATLAB Software R2015b*. MathWorks Inc.: Natick, MA, USA; 2015.
(22) IEEE Distribution Test Feeders [Online]. Available: http://ewh.ieee.org/soc/pes/dsacom/test feeders/index.html. Accessed on October 24, 2016.
(23) Kersting WH. The modeling and application of step voltage regulators. *Proceedings of IEEE/PES Power Systems Conference and Exposition*, (*PSCE '09*), 2009.

Tu Van Dao (Non-member) received the Engineer degree in power systems from Hanoi University of Science and Technology (HUST), Vietnam, in 2007. He worked at HUST as a Teaching Assistant and received the Master's degree in power systems there in 2009. From 2010 to 2013, he studied at Chulalongkorn University (CU), Thailand, and received the Ph.D. degree in electrical engineering. At present, he is working at CU as a Postdoctoral Research Fellow. His current research interests include renewable energy and smart grids.

Surachai Chaitusaney (Member) received the B. Eng. and M. Eng. degrees in electrical engineering from Chulalongkorn University (CU), Thailand, in 2000 and 2002, respectively, and the Ph.D. degree from The University of Tokyo, Japan, in 2007. He worked at the Energy Research Institute and the Center of Excellence in Power Technology, CU, from 2002 to 2004. At present, he is the Head of the Power Systems Research Laboratory (PSRL), CU. His research interests include renewable energy, distributed generation, and power systems planning, operation, and reliability.

Yasuhiro Hayashi (Member) received the B.Eng., M.Eng., and Dr.Eng. degrees in electrical engineering from Waseda University (WU), Tokyo, Japan, in 1989, 1991, and 1994, respectively. He worked as a Research Associate with Ibaraki University in 1994 and as an Associate Professor with the Department of Electrical and Electronics Engineering, Fukui University, in 2000. Since 2009, he has been a Professor with the Department of Electrical Engineering and Bioscience, WU. His current research interests include optimization of distribution system operation and planning, power system analysis, and load forecasting. Prof. Hayashi is a member of International Council on Large Electric Systems.

Hideo Ishii (Member) received the B.E., M.E. degrees in applied physics from the University of Tokyo in 1986 and 1988, respectively, and the Ph.D. degree from the same university in 1996. He joined Tokyo Electric Power Company (TEPCO) in 1988. He was a Visiting Scientist with the Massachusetts Institute of Technology, USA, from 1989 to 1991. He is now a Professor and Senior Researcher with the Advanced Collaborative Research Organization for Smart Society (ACROSS), Waseda University.